

# SwitchX- Gmin-Gmax Switching for Energy-Efficient and Robust Implementation of Binary Neural Networks on Memristive Xbars

Abhiroop Bhattacharjee, and Priyadarshini Panda  
Department of Electrical Engineering, Yale University, USA

**Abstract**—Memristive crossbars can efficiently implement *Binarized Neural Networks* (BNNs) wherein the weights are stored in high-resistance states (HRS) and low-resistance states (LRS) of the synapses. We propose *SwitchX* mapping of weights onto crossbars such that the power consumed by the crossbars and the impact of crossbar non-idealities, that lead to degradation in computational accuracy, are minimized. Essentially, *SwitchX* maps the binary weights in such manner that the crossbar comprises of more HRS than LRS synapses. Increased HRS in a crossbar will decrease the overall output dot-product current and thus lead to power savings. Interestingly, BNNs mapped onto crossbars with *SwitchX* also exhibit better robustness against adversarial attacks than the corresponding software BNN baseline as well as the standard crossbar mapped BNNs. Finally, we combine *SwitchX* with state-aware training (that further increases the feasibility of HRS states during weight mapping) to boost the robustness and energy-efficiency of BNN on hardware. We find that this approach yields stronger defense against adversarial attacks than Adversarial training, a state-of-the-art software defense. We perform experiments using benchmark datasets (CIFAR-100 & CIFAR-10) and show that *SwitchX* combined with state-aware training can yield upto  $\sim 35\%$  improvements in clean accuracy and  $\sim 6 - 16\%$  in adversarial accuracies against conventional BNNs on a  $32 \times 32$  crossbar, while gaining  $\sim 22\%$  savings in overall crossbar power consumption.

**Index Terms**—Binarized neural network, memristive crossbar, switched-mapping, adversarial robustness

## I. INTRODUCTION

Memristive crossbars have received significant focus for their ability to realize *Deep Neural Networks* (DNNs) by efficiently performing *Multiply-and-Accumulate* (MAC) operations using analog dot-products [1]–[3]. These systems have been realized using a wide range of emerging technologies such as, *Resistive RAM* (ReRAM), *Phase Change Memory* (PCM) and *Spintronic* devices [4]–[6]. These devices exhibit high on-chip storage density, non-volatility, low leakage and low-voltage operation and thus, enable compact and energy-efficient implementation of DNNs [7], [8].

In the recent years, *Binarized Neural Networks* (BNNs) have emerged as efficient and reasonably accurate low-precision models to implement DNNs. BNNs consist of binary synaptic weights, *viz.*  $\{-1, 1\}$ . The binarization enables lower computational complexity and power consumption for MAC operations. BNNs are crossbar-friendly in the sense that they can be implemented on crossbars in the manner shown in Fig. 2 (a). Here, the binarized weights are programmed as conductances of the synaptic devices at the cross-points. A weight value of

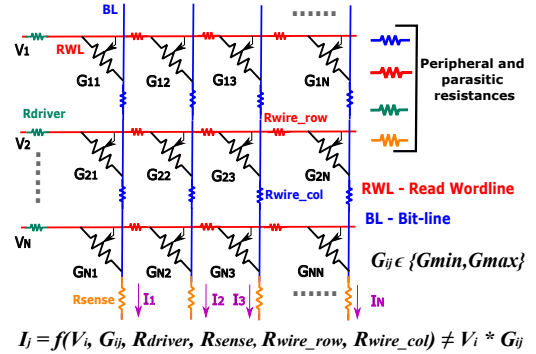


Fig. 1. An  $N \times N$  crossbar array with the various resistive non-idealities marked. The non-idealities lead to imprecise dot-product currents and that manifests as accuracy degradation when DNNs are evaluated on crossbars

‘+1’ corresponds to a *Low Resistance State* (LRS) while that of ‘-1’ corresponds to a *High Resistance State* (HRS). During inference, the activations of BNNs are fed into each row  $i$  of the crossbar as analog voltages (generated using Digital-to-Analog Converters (DACs)). As per Ohm’s Law, the voltages interact with the device conductances at the cross-points  $G_{ij}$  and produce a current. Consequently, by Kirchhoff’s current law, the net output current sensed at each column  $j$  is the sum of currents through each device, *i.e.*  $I_j = \sum_{i=1}^N G_{ij} * V_i$ . Owing to low leakage of the memristive devices, the dot-product operations in the crossbars constitute a significant portion of the chip power, especially for low-precision neural networks like BNNs [9], [10]. More number of LRS states on a crossbar array would result in higher dot-product output current that will lead to higher power consumption. In other words, the weights of the BNN encoded as resistance states in crossbars have a significant impact on the power consumed by the crossbars [9]. Therefore in this paper, to improve energy-efficiency of crossbars, we map the binarized weights in a way such that the number of HRS states always dominate the crossbar array resulting in reduced power. We term this as *SwitchX* based mapping of weights onto crossbars (see Fig. 2 (b)).

It is known that resistive crossbars possess non-idealities such as, interconnect parasitics, process variations in the synaptic devices, driver and sensing resistances, etc. [8], [11]. These non-idealities result in imprecise dot-product currents causing accuracy degradation when DNNs are mapped onto crossbars. In recent work [12], the authors have shown that the

crossbar non-idealities while degrading performance, improve the adversarial attack resilience of hardware-mapped DNNs in comparison to baseline software DNNs. Adversarial attacks are structured, yet, small perturbations on the input, that fool a DNN causing high confidence misclassification. This vulnerability severely limits the deployment and potential safe-use of DNNs for real world applications [13], [14]. In [14], [15], the authors show that hardware optimization techniques, such as, quantization and compression can be leveraged to improve adversarial robustness of DNNs in addition to energy-efficiency. In this work, we show that *SwitchX* mapping of BNNs onto crossbars interfere with hardware non-idealities to yield benefits in terms of power savings and adversarial robustness as compared to normally mapped BNNs.

**Contributions:** In summary, the key contributions of this work are as follows:

- 1) We comprehensively analyse how *SwitchX* mapping of binarized weights onto crossbars causes improved energy-efficiency of crossbar arrays and reduces the impact of crossbar non-idealities, which manifests as increase in the robustness of the mapped networks.
- 2) We carry out experiments on a state-of-the-art network (VGG16) [16] using benchmark datasets (CIFAR-100 & CIFAR-10) [17]. We propose a graphical approach via plotting *robustness maps* to evaluate the adversarial robustness of BNNs on  $16 \times 16$  and  $32 \times 32$  crossbars and perform a fair comparison between *SwitchX* and Normal Mapping.
- 3) We find that *SwitchX* approach when combined with state-aware training (explained in Section II-D) increases the feasibility of higher HRS mapping. This significantly boosts the robustness (both clean and adversarial accuracies) of the mapped BNNs. Further, *SwitchX* combined with state-aware training outperforms the case when *SwitchX* is combined with Adversarial training, a state-of-the-art software defense against adversarial attacks.
- 4) Apart from robustness benefits, we also show that the above approach can lead to significant power savings ( $\sim 22\%$  for  $32 \times 32$  crossbar) with respect to normally mapped BNNs on crossbars.

## II. BACKGROUND AND METHODOLOGY

### A. Memristive Crossbars and their non-idealities

Memristive crossbar arrays have been employed to implement *Matrix-Vector-Multiplications* (MVMs) in an analog manner. Crossbars (Fig. 1) consist of 2D arrays of synaptic devices, *Digital-to-Analog Converters* (DAC), *Analog-to-Digital Converters* (ADC) and a write circuit. The synaptic devices at the cross-points are programmed to a particular value of conductance (either  $G_{MIN}$  or  $G_{MAX}$  for a BNN). The MVM operations are performed by converting the digital inputs to the BNN into analog voltages on the *Read Wordlines* (RWLs) using DACs, and sensing the output current flowing through the bitlines (BLs) using the ADCs [8]. For an ideal crossbar, if  $V_{in}$  is the input voltage vector,  $I_{out_{ideal}}$  is the output current vector and  $G_{ideal}$  is the conductance matrix, then:

$$I_{out_{ideal}} = V_{in} * G_{ideal} \quad (1)$$

**Non-idealities and equivalent conductance matrix:** The analog nature of the computation leads to various non-idealities resulting in errors in the computation of MVMs. These include various linear resistive non-idealities in the crossbars. Fig. 1 shows the equivalent circuit for a crossbar array accounting for various peripheral and parasitic non-idealities ( $R_{driver}$ ,  $R_{wire\_row}$ ,  $R_{wire\_col}$  and  $R_{sense}$ ) modelled as parasitic resistances. The cumulative effect of all the non-idealities results in the deviation of the output current from its ideal value (*i.e.*, equation 1), resulting in an  $I_{out_{non-ideal}}$  vector. The relative deviation of  $I_{out_{non-ideal}}$  from its ideal value is measured by *non-ideality factor* (NF) [11] as:

$$NF = (I_{out_{ideal}} - I_{out_{non-ideal}}) / I_{out_{ideal}} \quad (2)$$

Thus, NF is a direct measure of crossbar non-idealities, *i.e.* increased non-idealities induce a greater value of NF, affecting the accuracy of the BNN mapped onto them [8], [11], [18].

From Fig. 2(a), once the binarized weights of a BNN are mapped to obtain  $G_{ideal}$ , we take into account the resistive non-idealities of the crossbar and convert  $G_{ideal}$  into  $G_{non-ideal}$  using circuit laws (*Kirchoff's laws* and *Ohm's law*) and linear algebraic operations following previous works [8], [18]. This completes the mapping of the weights of the BNN onto a non-ideal crossbar instance. Thus, we have:

$$I_{out_{non-ideal}} = V_{in} * G_{non-ideal} \quad (3)$$

Note, in this work, we carry out experiments on memristive crossbars with an ON/OFF ratio of 10 (*i.e.*,  $R_{MIN} = 20k\Omega$  and  $R_{MAX} = 200k\Omega$ ), having the resistive non-idealities as follows:  $R_{driver} = 1k\Omega$ ,  $R_{wire\_row} = 5\Omega$ ,  $R_{wire\_col} = 10\Omega$  and  $R_{sense} = 1k\Omega$ . We employ a framework in *PyTorch* [19] similar to *RxNN* [8], to map the BNNs onto crossbars and investigate the cumulative impact of the resistive non-idealities and *SwitchX*-mapping (explained in Section II-B) on the robustness of neural networks.

### B. SwitchX mapping

In the baseline or Normal Mapping of BNNs onto crossbars, '+1' weights are mapped to  $G_{MAX}$  or LRS and '-1' to  $G_{MIN}$  or HRS as shown in Fig. 2(a)). To reduce the power consumption due to MVM operations in a crossbar array, we perform switched-mapping of the weights of a BNN onto crossbars, termed as *SwitchX*. As shown in Fig. 2(b), we compute the mean of the binarized weight matrix of the BNN to be mapped onto a crossbar instance. If the mean is positive-valued, we switch the mapping with '+1' values to HRS states and '-1' values to LRS states. If mean is negative-valued, we don't perform any switching and conduct Normal Mapping (Fig. 2(a)). This approach ensures that the proportion of HRS states in a crossbar array is always higher when mapping BNN weights. As noted in Fig. 2(b), the ideal conductance matrix  $G_{ideal}$  obtained from the switched mapping is again converted into  $G_{non-ideal}$  taking the crossbar non-idealities into account.

**Inference during SwitchX:** The software model weights of a BNN are centered around zero, *i.e.* [-1, 1]. In crossbars,

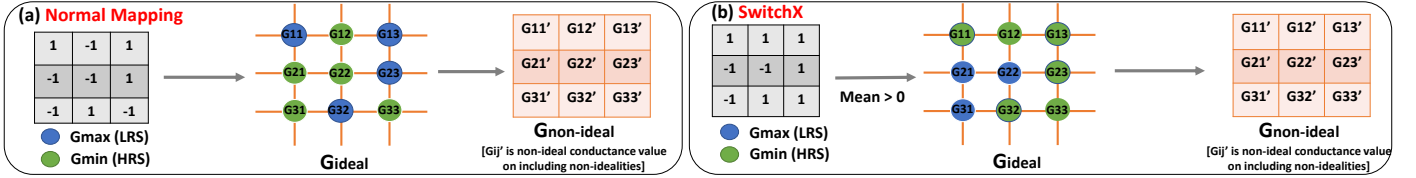


Fig. 2. (a)-(b) Pictorial representation of Normal Mapping and *SwitchX* approaches respectively showing mapping of a 3x3 binary weight matrix on 3x3 crossbar with non-idealities. In the case of Normal Mapping, '+1's are mapped to LRS states and '-1's are mapped to HRS states to obtain  $G_{ideal}$ . In the case of *SwitchX*, the mapping depends on the mean of the weight matrix. If mean  $< 0$ , then the process is similar to Normal Mapping. If mean  $> 0$ , then '+1's are mapped to HRS and '-1's to LRS. This ensures that HRS states are always in majority, thereby reducing the dot-product current and hence, the power.

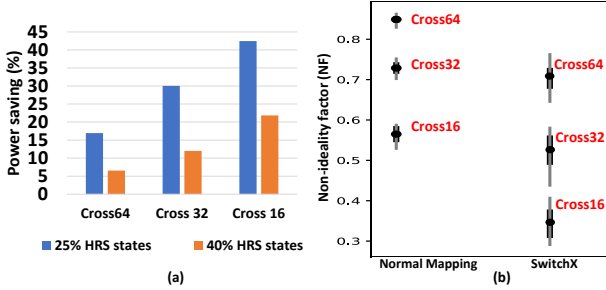


Fig. 3. (a) Plot showing power savings on various crossbar sizes with *SwitchX* mapping; (b) Box Plot of error bars to show variations in NF for various crossbar sizes in case of Normal Mapping and *SwitchX* mapping

the weights of a model are mapped onto  $[G_{MIN}, G_{MAX}]$  which is a skewed range. To conduct accurate inference, we need to perform some analytical treatment to ensure that the trained software weights after being mapped to conductance values still remain centered around zero, *i.e.*  $[-\frac{(G_{MAX}-G_{MIN})}{2}, \frac{(G_{MAX}-G_{MIN})}{2}]$ . This is generally done by employing opamp-based current generator and subtractor circuit modules to the columns of the crossbar [20], [21]. In *SwitchX*, based on the value of mean, the analytical operations are governed by equations (4) & (5).

For mean  $< 0$ ,

$$\sum a_i * w_{ij} = \sum V_i * G_{ij} - \frac{(G_{MAX} + G_{MIN})}{2} * \sum V_i \quad (4)$$

Note, the above is also true for normally mapping a BNN irrespective of the value of mean [20].

For mean  $> 0$ ,

$$\sum a_i * w_{ij} = -[\sum V_i * G_{ij} - \frac{(G_{MAX} + G_{MIN})}{2} * \sum V_i] \quad (5)$$

**Trends for non-ideality factor:** Fig. 3(b) shows the variation in NF for different crossbar sizes for a given binary weight matrix with higher proportion of '+1' values (mean  $> 0$ ) and a given set of input voltages. It is observed that the non-ideality factor increases with increasing crossbar size (16x16 to 64x64). Further for a given crossbar size, *SwitchX* results in a decrease in the value of NF with respect to the case of Normal Mapping. This occurs because *SwitchX* increases the effective resistance of a crossbar array, thereby minimizing the effect of interconnect parasitic resistances, by increasing the proportion of HRS states. This implies that when BNNs are mapped onto crossbars via *SwitchX* approach, the interference of non-idealities on MVM operations would be minimised which would cause lesser accuracy degradation, in addition to power savings.

**Trends for crossbar-power:** Fig. 3(a) shows a plot of the power savings observed when a binary weight matrix with

higher proportion of '+1' values are mapped onto crossbars of sizes 16x16, 32x32 and 64x64. The case of '25% HRS states' implies that 25% of the values in the BNN weight matrix are '-1' while, '40% HRS states' implies that 40% of the values are '-1', *i.e.* the weight matrix is less skewed than the former. We find that the power savings ( $\sim 17\% - 45\%$ ) increase when the distribution of weights is more skewed for different crossbar sizes. A more skewed distribution would imply greater proportion of HRS states on switched-mapping, thereby translating into greater power savings. Further, this would also imply greater reduction in non-ideality factor since a more skewed weight matrix would result in the increase of the overall crossbar resistance.

### C. Adversarial Attacks and Defense

Neural networks are vulnerable to adversarial attacks in which the model gets fooled by applying precisely calculated small perturbations on the input [14]. Goodfellow et al. [22] proposed *Fast Gradient Sign Method* (FGSM) to generate adversarial attacks ( $X_{adv}$ ) by linearization of the loss function ( $L$ ) of the trained models with respect to the input ( $X$ ) as shown in equation (6).

$$X_{adv} = X + \epsilon * \text{sign}(\nabla_x L(\theta, X, y_{true})) \quad (6)$$

Here,  $y_{true}$  is the true class label for the input  $X$ ;  $\theta$  denotes the model parameters (weights, biases etc.). The quantity  $\Delta = \epsilon * \text{sign}(\nabla_x L(\theta, X, y_{true}))$  is the net perturbation which is controlled by  $\epsilon$ . It is noteworthy that gradient propagation is a crucial step in unleashing an adversarial attack. Furthermore, the contribution of gradient to  $\Delta$  would vary for different layers of the network depending upon the activations [14]. In addition to FGSM-based attacks, multi-step variants of FGSM, such as *Projected Gradient Descent* (PGD) [23] have also been proposed that cast stronger attacks.

To build resilience against against small adversarial perturbations, defense mechanisms such as gradient masking or obfuscation [24] have been proposed. Such methods construct a model devoid of useful gradients, thereby making it difficult to create an adversarial attack. Furthermore, adversarial training [22], [23], [25], [26] is the state-of-the-art and strongest-known software defenses against adversarial attacks. Here, the training dataset is augmented with adversarial examples so that the network learns to predict them correctly. The authors in [12] have also shown that hardware non-idealities can intrinsically lead to defense via gradient obfuscation against adversarial perturbations, thereby making a neural network on hardware adversarially robust than baseline software models.

In this work, we explore how *SwitchX*, apart from yielding energy-efficiency and computational accuracy benefits to a BNN on hardware, can also yield adversarial robustness when compared with Normal Mapping of BNN weights onto crossbars. Furthermore, we show that when *SwitchX* is combined with state-aware training of BNN (discussed in Section II-D), it intrinsically unleashes even stronger defense on hardware than adversarial training.

#### D. Experiments

We conduct experiments on state-of-the-art VGG16 BNN architecture with benchmark datasets- CIFAR-10 & CIFAR-100. After training the BNNs on software, we launch FGSM and PGD attacks by adding adversarial perturbations to the clean test inputs and record the adversarial accuracies in each case. This forms our baseline software models (first two rows in TABLE I).

**State-aware training:** In normal scenario, the binarization of weights during software-training occurs with respect to a threshold ( $\delta$ ) value of 0.0. That is, a weight value greater (or lesser) than 0.0 is quantized as ‘+1’ (or ‘-1’), respectively. State-aware training is a method to make the distribution of binarized weights across a channel more skewed [9]. In this approach, the threshold ( $\delta$ ) is a hyperparameter assuming a positive value when there are more negative weights in a channel and a negative value otherwise. The weights are now quantized according to the new threshold value (in our experiments, we consider  $|\delta| = 1e - 3$ ). Subsequently, *SwitchX* based mapping on such networks will further increase the proportion of HRS states in the crossbar instances (resulting in reduction of power and non-ideality factor). State-aware training on VGG16 BNN using CIFAR-10 dataset yields a baseline software model as shown in TABLE I (third row). We extensively analyse the benefits of this approach in the upcoming sections.

**Modes of adversarial attack:** For the adversarial attacks (FGSM/PGD) on the crossbar-mapped models of the BNNs in order to assess robustness, we consider two modes - (a) *Software-inputs-on-hardware (SH) mode* where, the adversarial perturbations for each attack are created using the software-based baseline’s loss function and then added to the clean input that yields the adversarial input. The generated adversaries are then fed to the crossbar-mapped BNN. (b) *Hardware-inputs-on-hardware (HH) mode* where, the adversarial inputs are generated for each attack using the loss from the crossbar-based hardware models. It is evident that HH perturbations will incorporate the intrinsic hardware non-idealities and thus will cast stronger attacks than SH.

Note, all upcoming experiments are performed on crossbar sizes of  $16 \times 16$  or  $32 \times 32$  with the specifications given in Section II-A.

### III. RESULTS AND DISCUSSION

#### A. Robustness analysis

Earlier approaches to quantify adversarial robustness of neural networks have been based on *Adversarial Loss (AL)* metric which is the difference between the clean accuracy and the adversarial accuracy for a given value of  $\epsilon$  [12], [14], [15].

TABLE I  
BASELINE SOFTWARE MODELS USING BNN BASED ON VGG16 NETWORK WITH CIFAR-10 AND CIFAR-100 DATSETS SUBJECTED TO FGSM ATTACK

Model	Clean Accuracy	Adversarial accuracies					
		0.05	0.1	0.15	0.2	0.25	0.3
BNN with CIFAR-100	55.04	15.97	13.29	11.51	10.01	8.82	7.98
BNN with CIFAR-10	88.92	44.63	39.81	35.87	32.7	30.58	28.17
BNN with CIFAR-10 with state-aware training ( $ \delta  = 1e - 3$ )	87.55	46.61	40.63	35.64	31.82	28.86	26.38

A reduction in the value of AL is said to improve the adversarial robustness of the network. However, AL is not always a suitable metric for the assessment of robustness since reduction in AL does not convey whether the cause is a decrease in clean accuracy or an increase in adversarial accuracy or both. For instance, while evaluating a network with CIFAR-10 dataset, we find the clean and the adversarial accuracies (for a particular  $\epsilon$ ) to be 10% each. Then the value of AL is zero implying that the network is exceptionally robust. However, this is absurd since a 10% accuracy is random for CIFAR-10 dataset implying that the network is arbitrarily predicting and is not trained.

In this work, we evaluate robustness of the mapped BNNs on crossbars graphically as shown in Fig. 4 and Fig. 5. For a specific mode of attack (SH or HH) and a given crossbar size, we plot  $\Delta$  *Clean Accuracy*, the difference between clean accuracy of the mapped network in question and the corresponding clean accuracy of the software baseline, on the x-axis.  $\Delta$  *Adversarial Accuracy* (for a particular  $\epsilon$  value) which is the difference between the adversarial accuracy of the mapped network in question and the corresponding adversarial accuracy of the software baseline is plotted on the y-axis. We term this plot as a ‘*robustness map*’. The value of  $\Delta$  *Clean Accuracy* is always negative since BNNs when mapped on hardware suffer accuracy loss owing to non-idealities. The region bounded by the line  $y = -x$  and the y-axis denotes that the absolute increase in the adversarial accuracy is higher than the absolute degradation in the clean accuracy. If a point lies in this region closer to the y-axis, it implies greater adversarial accuracy with lower clean accuracy loss and hence, greater robustness. Therefore, this is our *favourable region*. Likewise, the region bounded by the line  $y = x$  and the y-axis is where the mapped-network is highly vulnerable to adversarial attacks and hence, the *unfavourable region*. This approach to assess robustness of a network is comprehensive and accurate since, it takes into account the cumulative impact of both clean accuracy and adversarial accuracy (which is a strong function of the clean accuracy). Note, for all cases the circular points correspond to mappings on  $16 \times 16$  crossbars while the triangular points correspond to mappings on  $32 \times 32$  crossbars. Furthermore, the details pertaining to the baseline software models have been listed in TABLE I.

Fig. 4 shows the robustness maps for BNNs based on VGG16 network with CIFAR-100 dataset for both SH and HH modes of attack. Fig. 4(a) and Fig. 4(b) pertain to FGSM attack with  $\epsilon$  varying from 0.05 to 0.3 with step size of 0.05. We find that *SwitchX* imparts greater clean accuracy ( $\sim 3\%$  for  $32 \times 32$

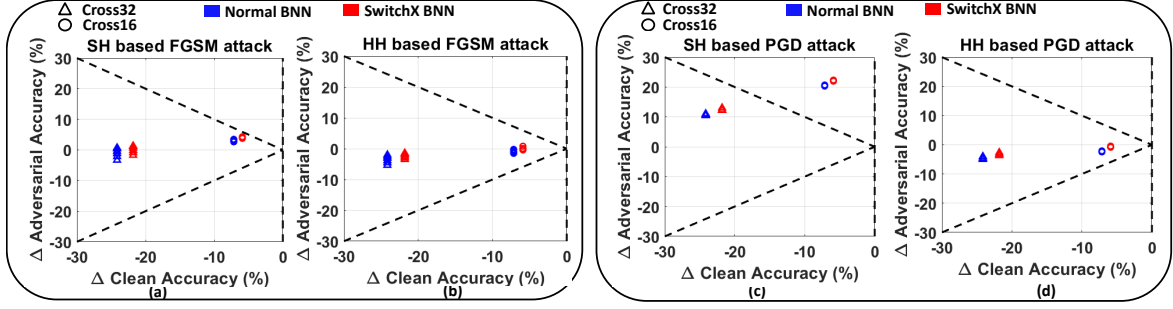


Fig. 4. (a)-(b) Robustness maps for VGG16 based BNN using CIFAR-100 dataset for SH and HH modes of FGSM attack respectively; (c)-(d) Robustness maps for VGG16 based BNN using CIFAR-100 dataset for SH and HH modes of PGD attack respectively

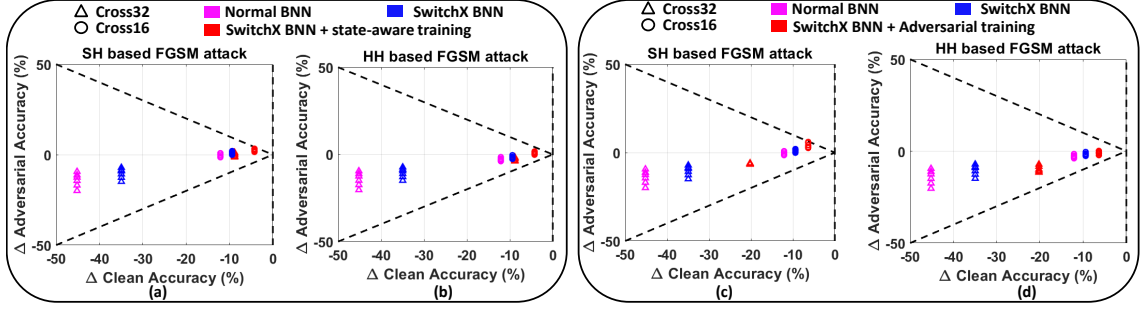


Fig. 5. (a)-(b) Robustness maps for VGG16 based BNN using CIFAR-10 dataset for SH and HH modes of FGSM attack respectively considering the case of *SwitchX* combined with state-aware training; (c)-(d) Robustness maps for VGG16 based BNN using CIFAR-10 dataset for SH and HH modes of FGSM attack respectively considering the case of *SwitchX* combined with adversarial training

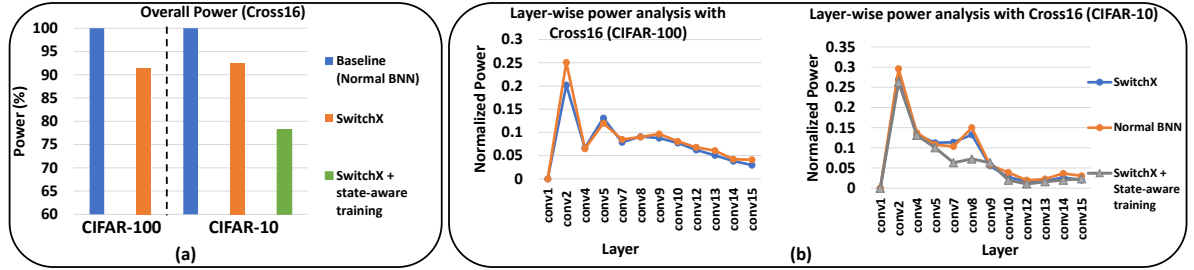


Fig. 6. (a) Plot showing power savings for standalone *SwitchX* as well as *SwitchX* combined with state-aware training with respect to the baseline of Normal BNN for  $16 \times 16$  crossbar; (b) Plot showing layer-wise power consumption for the different convolutional layers in the BNN using CIFAR-10 and CIFAR-100 datasets in case of mapping on  $16 \times 16$  crossbars

crossbar) as well as better adversarial accuracies on hardware for both modes of attack, with the points corresponding to *SwitchX* situated closer to the favourable region than the corresponding points for Normal Mapping. This is a consequence of the reduction in non-ideality factor in case of *SwitchX* with respect to Normal Mapping as discussed in Section II-A. Note, the points for  $32 \times 32$  crossbars are situated farther from the favourable region than the corresponding points for  $16 \times 16$  crossbars. This is owing to greater non-idealities that exist in case of a  $32 \times 32$  crossbar than a  $16 \times 16$  crossbar (Fig. 3(b)). We further observe that the points for *SwitchX BNN* for a given crossbar size are more closely packed than the corresponding points for Normal BNN. This implies that even on increasing the perturbation strength ( $\epsilon$ ), lesser adversarial loss is observed in case of *SwitchX BNN*.

Fig. 4(c) and Fig. 4(d) also present similar results but for a PGD attack with  $\epsilon$  varying from  $2/255$  to  $32/255$  with step size of  $2/255$ . In this case, the robustness is very high for SH mode of attack as compared to HH mode of attack, with

points corresponding to  $16 \times 16$  crossbars situated inside the favourable region. Similar to the case of FGSM attack, *SwitchX* outperforms a Normal BNN in terms of robustness for both modes of attack. Here, points for different  $\epsilon$  values, given a style of mapping and crossbar size, are more closely packed than the corresponding points of FGSM attack. This implies that hardware non-idealities interfere more with PGD attacks than FGSM attacks resulting in lesser accuracy degradation.

Fig. 5 shows the robustness maps for BNNs based on VGG16 network with CIFAR-10 dataset for both SH and HH modes of FGSM attack. Here, we find that there is a significant benefit in terms of improvement in clean accuracy due to *SwitchX* for a  $32 \times 32$  crossbar ( $\sim 10\%$ ) with respect to Normal Mapping. Similar to the case for CIFAR-100 dataset, we find that *SwitchX* outperforms a Normal BNN in terms of robustness for both modes of attack. Furthermore, we also analyse cases when *SwitchX* is combined with state-aware training as well as adversarial training. The results for FGSM attack are summarized:

1) *With Adversarial Training*: From Fig. 5(c) and Fig. 5(d), we find that *SwitchX* combined with adversarial training significantly boosts the robustness of the mapped BNN both in terms of clean as well as adversarial accuracy improvement. For  $16 \times 16$  crossbar, the points (in red) for different  $\epsilon$  lie in the close vicinity of the boundary of the favourable region while for  $32 \times 32$  crossbar, the rise in clean accuracy with respect to Normal BNN is very high ( $\sim 20\%$ ). Furthermore, given a style of mapping and crossbar size, the points for adversarial training are more closely packed than the corresponding points of standalone *SwitchX BNN* or Normal BNN, implying lesser accuracy losses on increasing perturbation strength of attack.

2) *With State-aware Training*: As discussed in Section II-D, state-aware mapping combined with *SwitchX* can lead to increase in the proportion of HRS states in the crossbar instances, and thus a reduction in the non-ideality factor of the crossbars. From Fig. 5(a) and Fig. 5(b), we find that this approach significantly boosts the robustness of the mapped BNN both in terms of clean as well as adversarial accuracy improvements. For both  $16 \times 16$  and  $32 \times 32$  crossbars, the points (in red) for different  $\epsilon$  lie in the close vicinity of the boundary of the favourable region. We find that for  $32 \times 32$  crossbar, the rise in clean and adversarial accuracies is so large that it becomes comparable to the case of standalone *SwitchX BNN* mapped on a smaller  $16 \times 16$  crossbar. Overall, we find the rise in clean and adversarial accuracies is  $\sim 35\%$  and  $\sim 6 - 16\%$  greater than Normal BNN, respectively. In this case also, the points for different  $\epsilon$  values, given a style of mapping and crossbar size, are more closely packed than the corresponding points of standalone *SwitchX BNN* or Normal BNN, implying lesser accuracy losses on increasing perturbation strength of attack. Interestingly, we find that this approach emerges as a stronger defense against adversarial attacks than *SwitchX* combined with adversarial training (a state-of-the-art software defense), the defensive action being more pronounced for larger crossbar sizes ( $32 \times 32$  in Fig. 5(a) and Fig. 5(b)).

### B. Crossbar power analysis

From Fig. 6(a) (data shown for a  $16 \times 16$  crossbar), we find that standalone *SwitchX* approach leads to  $\sim 9\%$  power-savings on an average with respect to Normal BNN for a VGG16 network with CIFAR-100 dataset. While for CIFAR-10 dataset, there is  $\sim 8\%$  power saving for standalone *SwitchX*, it increases to  $\sim 21\%$  when *SwitchX* is combined with state-aware training. Furthermore, on carrying out similar experiments on  $32 \times 32$  crossbars, we obtain  $\sim 22\%$  power savings on combining *SwitchX* with state-aware training. Fig. 6(b) shows the layer-wise normalized average power consumption by the network with CIFAR-100 and CIFAR-10 dataset. We find that overall for each convolutional layer of the network, the power consumed by the *SwitchX BNN* is lesser than the Normal BNN. Furthermore, this reduction becomes even more significant between ‘conv7’ and ‘conv9’ layers when *SwitchX* is combined with state-aware training (data shown for CIFAR-10 dataset). This result is in accordance with Fig. 3(a) which shows that the power savings on crossbar arrays increase significantly when the HRS-LRS state-distribution becomes more skewed.

## IV. CONCLUSION

In this work, we propose *SwitchX* based mapping of binary weights onto crossbars in such a manner that a crossbar comprises of more HRS than LRS synapses. This ensures that the analog dot-product currents in crossbars during inference are minimized, thereby saving crossbar power. We perform a comprehensive analysis on crossbar arrays comprising of resistive non-idealities, whereby *SwitchX* reduces the overall impact of non-idealities during inference. This effect manifests as reduced accuracy losses and increased robustness against adversarial attacks for BNNs mapped onto crossbars. We also combine *SwitchX* with state-aware training that further increases the feasibility of HRS states during weight mapping to boost power savings as well as robustness.

## ACKNOWLEDGEMENT

This work was supported in part by the National Science Foundation (Grant#1947826), and the Amazon Research Award.

## REFERENCES

- [1] C. D. Schuman, T. E. Potok, R. M. Patton, J. D. Birdwell, M. E. Dean, G. S. Rose, and J. S. Plank, “A survey of neuromorphic computing and neural networks in hardware,” *arXiv preprint arXiv:1705.06963*, 2017.
- [2] H.-S. P. Wong, H.-Y. Lee, S. Yu, Y.-S. Chen, Y. Wu, P.-S. Chen, B. Lee, F. T. Chen, and M.-J. Tsai, “Metal-oxide rram,” *Proceedings of the IEEE*, vol. 100, no. 6, pp. 1951–1970, 2012.
- [3] M. Sharad, G. Panagopoulos, and K. Roy, “Spin neuron for ultra low power computational hardware,” in *70th Device Research Conference*. IEEE, 2012, pp. 221–222.
- [4] W.-H. Chen, W.-S. Khwa, J.-Y. Li, W.-Y. Lin, H.-T. Lin, Y. Liu, Y. Wang, H. Wu, H. Yang, and M.-F. Chang, “Circuit design for beyond von neumann applications using emerging memory: From nonvolatile logics to neuromorphic computing,” in *2017 18th International Symposium on Quality Electronic Design (ISQED)*. IEEE, 2017, pp. 23–28.
- [5] A. Sengupta, Y. Shim, and K. Roy, “Proposal for an all-spin artificial neural network: Emulating neural and synaptic functionalities through domain wall motion in ferromagnets,” *IEEE transactions on biomedical circuits and systems*, vol. 10, no. 6, pp. 1152–1160, 2016.
- [6] D. Fan, Y. Shim, A. Raghunathan, and K. Roy, “Stt-snn: A spin-transfer-torque based soft-limiting non-linear neuron for low-power artificial neural networks,” *IEEE Transactions on Nanotechnology*, vol. 14, no. 6, pp. 1013–1023, 2015.
- [7] A. Ankit, I. E. Hajj, S. R. Chalamalasetti, G. Ndu, M. Foltin, R. S. Williams, P. Faraboschi, W.-m. W. Hwu, J. P. Strachan, K. Roy *et al.*, “Puma: A programmable ultra-efficient memristor-based accelerator for machine learning inference,” in *Proceedings of the Twenty-Fourth International Conference on Architectural Support for Programming Languages and Operating Systems*, 2019, pp. 715–731.
- [8] S. Jain, A. Sengupta, K. Roy, and A. Raghunathan, “Rxn: A framework for evaluating deep neural networks on resistive crossbars,” *IEEE Transactions on Computer-Aided Design of Integrated Circuits and Systems*, 2020.
- [9] Y. He, Y. Wang, X. Zhao, H. Li, and X. Li, “Towards state-aware computation in rram neural networks,” in *2020 57th ACM/IEEE Design Automation Conference (DAC)*. IEEE, 2020, pp. 1–6.
- [10] M.-F. Chang, A. Lee, P.-C. Chen, C. J. Lin, Y.-C. King, S.-S. Sheu, and T.-K. Ku, “Challenges and circuit techniques for energy-efficient on-chip nonvolatile memory using memristive devices,” *IEEE Journal on Emerging and Selected Topics in Circuits and Systems*, vol. 5, no. 2, pp. 183–193, 2015.
- [11] I. Chakraborty, M. F. Ali, D. E. Kim, A. Ankit, and K. Roy, “Geniex: A generalized approach to emulating non-ideality in memristive xbars using neural networks,” *arXiv preprint arXiv:2003.06902*, 2020.
- [12] A. Bhattacharjee and P. Panda, “Rethinking non-idealities in memristive crossbars for adversarial robustness in neural networks,” *arXiv preprint arXiv:2008.11298*, 2020.

- [13] N. Carlini, A. Athalye, N. Papernot, W. Brendel, J. Rauber, D. Tsipras, I. Goodfellow, A. Madry, and A. Kurakin, "On evaluating adversarial robustness," *arXiv preprint arXiv:1902.06705*, 2019.
- [14] P. Panda, "Quanos-adversarial noise sensitivity driven hybrid quantization of neural networks," *arXiv preprint arXiv:2004.11233*, 2020.
- [15] P. Panda, I. Chakraborty, and K. Roy, "Discretization based solutions for secure machine learning against adversarial attacks," *IEEE Access*, vol. 7, pp. 70 157–70 168, 2019.
- [16] K. Simonyan and A. Zisserman, "Very deep convolutional networks for large-scale image recognition," *arXiv preprint arXiv:1409.1556*, 2014.
- [17] A. Krizhevsky, G. Hinton *et al.*, "Learning multiple layers of features from tiny images," 2009.
- [18] S. Jain and A. Raghunathan, "Cxdnn: Hardware-software compensation methods for deep neural networks on resistive crossbar systems," *ACM Transactions on Embedded Computing Systems (TECS)*, vol. 18, no. 6, pp. 1–23, 2019.
- [19] A. Paszke, S. Gross, S. Chintala, G. Chanan, E. Yang, Z. DeVito, Z. Lin, A. Desmaison, L. Antiga, and A. Lerer, "Automatic differentiation in pytorch," 2017.
- [20] Y. Kim, W. H. Jeong, S. B. Tran, H. C. Woo, J. Kim, C. S. Hwang, K.-S. Min, and B. J. Choi, "Memristor crossbar array for binarized neural networks," *AIP Advances*, vol. 9, no. 4, p. 045131, 2019.
- [21] S. N. Truong and K.-S. Min, "New memristor-based crossbar array architecture with 50-% area reduction and 48-% power saving for matrix-vector multiplication of analog neuromorphic computing," *JSTS: Journal of Semiconductor Technology and Science*, vol. 14, no. 3, pp. 356–363, 2014.
- [22] I. J. Goodfellow, J. Shlens, and C. Szegedy, "Explaining and harnessing adversarial examples," *arXiv preprint arXiv:1412.6572*, 2014.
- [23] A. Madry, A. Makelov, L. Schmidt, D. Tsipras, and A. Vladu, "Towards deep learning models resistant to adversarial attacks," *arXiv preprint arXiv:1706.06083*, 2017.
- [24] N. Papernot, P. McDaniel, I. Goodfellow, S. Jha, Z. B. Celik, and A. Swami, "Practical black-box attacks against machine learning," in *Proceedings of the 2017 ACM on Asia conference on computer and communications security*, 2017, pp. 506–519.
- [25] A. Kurakin, I. Goodfellow, and S. Bengio, "Adversarial machine learning at scale," *arXiv preprint arXiv:1611.01236*, 2016.
- [26] H. Lee, S. Han, and J. Lee, "Generative adversarial trainer: Defense to adversarial perturbations with gan," *arXiv preprint arXiv:1705.03387*, 2017.